Decomposition of the Green's function using the Marchenko equation

Joeri Brackenhoff, Joost van der Neut, Kees Wapenaar, Delft University of Technology

SUMMARY

The Marchenko equation can be used to retrieve the Green's function at depth as a full function or decomposed into its up- and downgoing parts. We show that the equation can be rewritten to create a decomposition scheme that can decompose a full wavefield, that was recorded at depth, into its up- and downgoing parts. We show that this can be done without a smooth velocity model that the Marchenko scheme requires and without any knowledge of the medium properties that traditional decomposition methods require. Instead we only need a the reflection response and a wavefield that has been recorded at the surface due to a source at depth or (by using source-receiver reciprocity) that was measured down in a borehole due to a source at the surface. We also validate our results by comparing them to directly modeled up- and downgoing wavefields.

INTRODUCTION

In recent years the Marchenko equation has been utilized for seismic data processing and imaging. The method was first developed for seismic data processing and imaging by (Broggini et al., 2014) and further expanded in 2D/3D by (Wapenaar et al., 2014). They showed that the Marchenko equation allows the retrieval of Green's function at any virtual receiver location in a medium as a full function or as its up- and downgoing components. The Green's function at depth can be used for various purposes, such as the elimation of multiples (Meles et al., 2015) or imaging of the subsurface (Ravasi et al., 2016). The Marchenko scheme requires only the reflection response measured at a single recording surface of the medium and an estimation of the first arrival at the virtual receiver location. This is in contrast to other theoretical wave methods, such as time-reverse migration, which require a full recording surface around the medium. However, the Marchenko equation can also be used for other applications, such as wavefield decomposition. Decomposition is the practice of separating a full wavefield into its up- and downgoing parts. These one-way wavefields can be used for various purposes, including seismic imaging (Wapenaar et al., 2014). Decomposition can be applied to various types of data, such as using ocean cable bottom data (Amundsen and Reitan, 1995), streamer data (Day et al., 2013) or down in boreholes (Mehta et al., 2007; Grobbe et al., 2015). Traditional decomposition methods require multicomponent data, meaning that both the particle velocity and pressure wavefields need to be measured. Using the Marchenko method we can use single component measurements to decompose the full wavefield into its up- and downgoing parts. In order to do this we require a reflection response without free-surface multiples of the medium of interest that has been recorded at the surface. This reflection response is the only knowledge we need of the actual medium. If we record a wavefield that contains up- and downgoing waves in the medium we
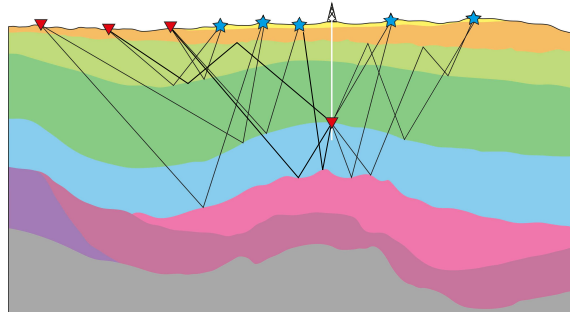
Figure 1: *Schematic view of a borehole containing a receiver. The receiver is located downhole in the borehole, while the sources are present at the surface. Several raypaths have been drawn to show the arrival of up- and downgoing events at the receiver. There are also several receivers at the surface that measure the reflection response of the medium below.*

can decompose the full wavefield. This is very useful for when a receiver is present in a borehole, which is illustrated in Fig.1. Sources at the surface create a wavefield that can measured by the receiver in the borehole. Because the receiver is downhole, it will measure both the up- and downgoing wavefields, which is illustrated in the figure by several raypaths. Furthermore, there are several receivers at the surface that measure the reflection response of the medium. Using this single receiver in this borehole and the reflection response, we can then decompose the wavefield that was measured down in the borehole. Alternatively there could also be a source present in the medium itself, either in the borehole or as a microseismic event. The receivers at the surface will measure the response of this source and by using source-receiver reciprocity we will receive the wavefield at depth, which can be decomposed as well. This scheme can be used without any knowledge of the physical parameters of the medium and without the need of an estimated first arrival that the Marchenko scheme would require.

THEORY

A Green's function is composed of upgoing waves and downgoing waves:

$$G(\mathbf{x}_E, \mathbf{x}, t) = G^+(\mathbf{x}_E, \mathbf{x}, t) + G^-(\mathbf{x}_E, \mathbf{x}, t), \quad (1)$$

where G is the full Green's function at time t at location $\mathbf{x}_E$ due to a source at location $\mathbf{x}$, G^+ is its downgoing component and G^- is its upgoing component. Using source-receiver reciprocity, the location of the source and receiver can be interchanged. For G this will produce the exact same wavefield. Using the Marchenko method and a reflection response these

Decomposition of the Green's function using the Marchenko equation

Green's functions can be retrieved as described in Wapenaar et al. (2014) and van der Neut et al. (2015). The important equations of these papers can be summarized as:

$$G^-(\mathbf{x}_E,\mathbf{x},t) + f_1^-(\mathbf{x},\mathbf{x}_E,t) = \{\mathcal{R}f_1^+\}(\mathbf{x},\mathbf{x}_E,t) \qquad (2)$$

$$G^+(\mathbf{x}_E,\mathbf{x},-t) - f_1^+(\mathbf{x},\mathbf{x}_E,t) = -\{\mathcal{R}^\star f_1^-\}(\mathbf{x},\mathbf{x}_E,t), \qquad (3)$$

where $\mathcal{R}$ indicates a space-time convolution with the reflection response and $\mathcal{R}^\star$ indicates a space-time convolution with the time-reversed reflection response. Note also that the downgoing Green's function is reversed in time. f_1^+ and f_1^- indicate the downgoing and upgoing focusing function at time t at location $\mathbf{x}$ which will focus downwards to location $\mathbf{x}_E$. Similarly to the Green's function the full focusing function can be constructed from the upgoing and downgoing components:

$$f_1(\mathbf{x},\mathbf{x}_E,t) = f_1^+(\mathbf{x},\mathbf{x}_E,t) + f_1^-(\mathbf{x},\mathbf{x}_E,t), \qquad (4)$$

The downgoing focusing function f_1^+ is defined as the inverse of the transmission response in a truncated medium, where there are no reflectors below the focusing location. Based on causality arguments, under specific circumstances, the focusing function and Green's function can be separated in time from each other through the use of a time gate. This is because all of the events of the focusing function arrive before the Green's function, with the exception of the first arrival. We define the time gate $\Theta^{-\varepsilon}$ which removes the Green's function but retains the focusing functions, with the exception of the first arrival of f_1^+. We also define the complement of $\Theta^{-\varepsilon}$, which is the time gate $\Psi^{+\varepsilon}$, which retains the Green's functions, but removes the focusing functions except for the first arrival of f_1^+. The time gates are symmetrical in time so time-reversal does not affect the gates. Note that due to the band-limited character of seismic data a small time shift needs to be applied to the windows in order to ensure that part of the wavelet is not removed. This is indicated by the ε, which indicates we shift the time gate limit by a small amount ε. For Θ this shift is backwards $(-\varepsilon)$ so the direct arrival is removed and for Ψ the shift is forward $(+\varepsilon)$ so the direct arrival is retained. We now apply $\Psi^{+\varepsilon}$ to eqn. 2 to remove the focusing function $(\Psi^{+\varepsilon}f_1^- = 0)$ and apply time-reversal:

$$G^-(\mathbf{x}_E,\mathbf{x},-t) = \{\mathcal{Z}\Psi^{+\varepsilon}\mathcal{R}f_1^+\}(\mathbf{x},\mathbf{x}_E,t) \qquad (5)$$

In eqn. 5, we have introduced a time-reversal operator $\mathcal{Z}$ so that the focusing function is forward in time. This was done to make the derivation easier later on. We also apply $\Theta^{-\varepsilon}$ to eqn. 2 to remove the Green's function $(\Theta^{-\varepsilon}G = 0)$:

$$f_1^-(\mathbf{x},\mathbf{x}_E,t) = \{\Theta^{-\varepsilon}\mathcal{R}f_1^+\}(\mathbf{x},\mathbf{x}_E,t) \qquad (6)$$

The result of eqn. 6 can be inserted into eqn. 3 to obtain:

$$G^+(\mathbf{x}_E,\mathbf{x},-t) = \{(\mathbf{I} - \mathcal{R}^\star\Theta^{-\varepsilon}\mathcal{R})f_1^+\}(\mathbf{x},\mathbf{x}_E,t) \qquad (7)$$

When eqn. 5 and eqn. 7 are added together we arrive at an expression for the full Green's function:

$$G(\mathbf{x}_E,\mathbf{x},-t) = \{(\mathbf{I} - (\mathcal{R}^\star\Theta^{-\varepsilon}\mathcal{R} - \mathcal{Z}\Psi^{+\varepsilon}\mathcal{R}))f_1^+\}(\mathbf{x},\mathbf{x}_E,t), \qquad (8)$$

which can be solved using inversion. Alternatively eqn. 8 can be solved by the following Neumann expansion:

$$f_1^+(\mathbf{x},\mathbf{x}_E,t) = \sum_{k=0}^{\infty}(\mathcal{R}^\star\Theta^{-\varepsilon}\mathcal{R} - \mathcal{Z}\Psi^{+\varepsilon}\mathcal{R})^k G(\mathbf{x}_E,\mathbf{x},-t) \qquad (9)$$

Eqn. 9 demonstrates how the focusing function can be retrieved from the full Green's function, which can then be inserted into eqn. 5 and eqn. 7 to obtain the upgoing and downgoing Green's functions. As can be seen by eqn. 9 the only requirements are a reflection response to generate the operator $\mathcal{R}$ and a measurement of the wavefield G. This means that no additional knowledge of the medium itself is required and a single component measurement is sufficient for decomposition. Also, because the input data of the first iteration is the measured wavefield, we do not need to model the first arrival, which the Marchenko scheme requires.

MODELING

In order to show the validity of our method we decompose a 1D wavefield. The model is shown in Fig.2-a and Fig.2-b. It contains both velocity and density variations. The reflection response of this model that is measured at the surface is shown in Fig.2-c. Using this model, we modeled a full Green's function at depth using a 1D code. The results can be found in Fig.2-d, which we will use for reference. Both positive and negative times are shown, but the Green's function only exists at the positive times because it is causal. Using another 1D code we also retrieve the transmission response at depth in a truncated medium, where there are no reflectors present below the receiver location. By inverting this transmission response, we get the downgoing focusing function (Wapenaar et al., 2014). The result is shown in Fig.2-e, which we will also use for reference. Notice that the first event in the focusing function is arriving at the negative time of the first arrival in the Green's function, but the amplitude of the direct arrival of the focusing function is higher. Except for the first arrival, all of the other events of the focusing function are located within the red dashed lines. The events of the Green's function are located outside of the lines. These lines indicate the limits of the time gates and show how the separation works that we used in the equations in the previous section. The coda of the focusing function is located entirely within the indicated limits (corresponding to $\Theta^{-\varepsilon}$) and the direct arrival and all events of the Green's function are located outside these limits (corresponding to $\Psi^{+\varepsilon}$. This shows how the two different types of wavefields can be separated.

We now use the full Green's function in Fig.2-d as the input using the indicated time gates along with the reflection response in Fig.2-c to show how the focusing function is constructed using eqn. 9. The first iteration will be the time-reversed Green's

Decomposition of the Green's function using the Marchenko equation
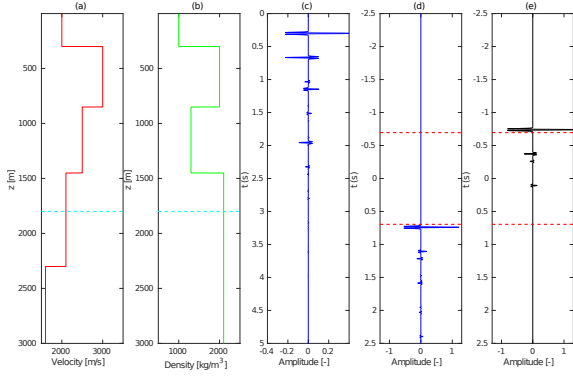
Figure 2: *(a) Velocity and (b) density of the 1D model. The depth of our receiver is indicated by the light blue dashed line. (c) The reflection response measured at the surface of the model in (a) and (b). (d) The Green's function response at the receiver. (e) The downgoing focusing function response at the receiver. The events in (c), (d) and (e) have all been convolved with a 30 Hz Ricker wavelet. The limits of the time gate $\Theta^{-\varepsilon}$ and $\Psi^{+\varepsilon}$ are indicated in dashed red. The results in (d) and (e) were obtained using 1D modeling codes and will be used for reference to validate the results.*

Figure 3: *Overview of the construction of the first update using eqn. 9. (a) The time-reversed version, $G(-t)$, of the Green's function from Fig.2-d. (b) The function from (a) convolved with the reflection response from Fig.2-c, $\mathscr{R}G(-t)$. (c) The time-reversed events outside the limits of the time gates in (b), $\mathscr{L}\Psi^{+\varepsilon}\mathscr{R}G(-t)$. (d) The results of the convolution with the time-reversed reflection response from Fig.2-c and the events within the limits of the time gates in (b), $\mathscr{R}^{\star}\Theta^{-\varepsilon}\mathscr{R}G(-t)$ (e) The full update as a result of substracting the events in (b) from the events in (d), $(\mathscr{R}^{\star}\Theta^{-\varepsilon}\mathscr{R} - \mathscr{L}\Psi^{+\varepsilon}\mathscr{R})G(-t)$. The time gate limits are indicated in dashed red.*

function, but subsequent iterations will be calculated by the terms in brackets and added to this first iteration. In this regard, each iteration can be seen as an update to the previous estimation. We will demonstrate how the update that is associated to the second iteration is constructed. The process for the first update is shown in Fig.3. First, we time-reverse the Green's function, which is shown in Fig.3-a. All the events are now at negative times and are still all outside the time gate limits. Because the events in the reflection response are all at positive times a convolution will shift the events backwards in time. The convolution of the reflection response and the time-reversed Green's function is shown in Fig.3-b. There are now several events inside the limits of the time gate and there are also some present outside the time gate at positive and negative times. Using the time gate we can separate these events from each other. We apply $\Psi^{+\varepsilon}$ to the events and time-reverse the results as shown in Fig.3-c. This is one half of the update in eqn. 9, $\mathscr{L}\Psi^{+\varepsilon}\mathscr{R}G(-t)$. Because these events are all outside the time gate limits they do not contribute to the desired events in the reconstructed focusing function, but are only meant to dampen the artifacts that should not be present. The only exception is the first arrival of the focusing function, which it does update, but is present outisde the limits of the time gate. If instead of $\Psi^{+\varepsilon}$ we apply $\Theta^{-\varepsilon}$ to the events in Fig.3-b and we apply a convolution with the time-reversed reflection response. We get the result shown in Fig.3-d. This is the other half of the update $\mathscr{R}^{\star}\Theta^{-\varepsilon}\mathscr{R}G(-t)$. This update contains events that are both inside and outside the limits of the time gate. It updates the events that should be present in the focusing function and also dampens the unwanted artifacts. By subtracting the results in Fig.3-c from the results in Fig.3-d, we get the full update as shown in Fig.3-e. If we were to add this result to the time-reversed Green's function in Fig.3-a, we see that the amplitude

of the direct arrival is increased, which it should as we can see from the reference data, and the other events in that function are damped. Furthermore, several events within the time gate limits are added. There are also events outside the time gate that are added, which should not be present. These events will be removed in subsequent iterations. Also not all of the amplitudes of the updates are strong enough to completely remove the artifacts. Several more updates will be required to retrieve the correct focusing function.

We show the construction of the focusing function in Fig.4, plotted against the iteration number. The updates are shown in black and the desired focusing function from Fig.2-e is plotted in dashed green over the updates for reference. The trace at iteration 0 is the time-reversed Green's function and the trace at iteration 1 is the result of the first trace after applying the update in Fig.3-e. As indicated several events are added. Additionally, there are also events that were already present and have their amplitude changed. The first arrival and several desired events are not strong enough yet and there are several artifacts added that should not be present. Subsequent updates fix these problems. The amplitudes of the desired events are all updated to be correct and the artifacts are removed. The amount of energy that is added and removed decreases with each iteration, indicating that the solution is converging. After about 8 iterations the updates are so small that they are no longer visible on the trace. When comparing the constructed focusing function to the desired one, we can see that they match very well. There are no strange events present in the focusing function and the desired events overlap. We can now use the retrieved focusing function in combination with eqn. 5 and 7 to see if the retrieved up- and downgoing waves are accurate.

Decomposition of the Green's function using the Marchenko equation
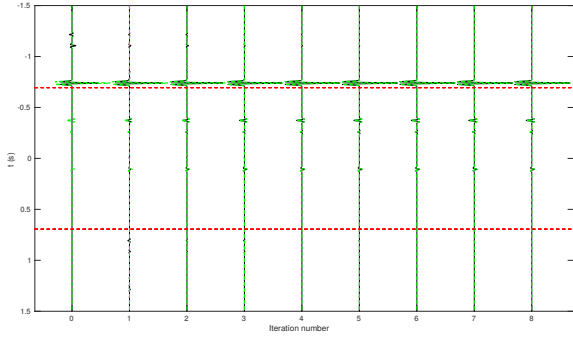
Figure 4: *Updates of the constructed focusing function against each update number. The black lines represent the focusing function per update. Over each update the desired focusing function from Fig.2-e is plotted in dashed green. The time gate limits are shown in dashed red.*

In Fig.5 we show the retrieved wavefields. In Fig.5-a we show the upgoing wavefield and in Fig.5-b we show the downgoing wavefield. The retrieved wavefields do not show any obvious errors and the amplitudes are all within the range of the original input. Using eqn. 1 we can see that the retrieved results should add up to the input data. This is done in Fig.5-c, where the dashed green trace is the input data and the solid black line is the summation of the traces of the previous two figures. Visually the two traces appear to have complete overlap. The first arrival of the downgoing wavefield should be the same as the one of the full Green's function. In the upgoing field there is no event present at the time of the first arrival in the downgoing field. To further prove the accuracy of the results, in Fig.5-d we show the error between the two traces in Fig.5-c. The result appears to be an empty trace. This shows that the retrieved amplitudes are so accurate that the errors are not visible on the trace, similar to the result we got on the retrieved and reference focusing function. The decomposition can accurately recover the up- and downgoing wavefield from a full wavefield using only the reflection response and the measured wavefield in the subsurface.

CONCLUSION AND DISCUSSION

We have shown that we can derive a decomposition scheme from the Marchenko equation. This decomposition scheme can decompose single component wavefield with accurate results. It does not require multicomponent recording or knowledge of the medium properties that other decomposition methods require. It also does not require an estimation of the first arrival from a smooth velocity model that the Marchenko method requires. The method does have its limitations. Unlike other decomposition methods it requires an reflection response and, like many other Marchenko based methods, it is very sensitive to errors in the reflection response. Furthermore, in order to use this method a measured wavefield is required and therefore either a downhole receiver needs to be present. The method could be used for other cases as well, such as when microseismic events are measured. If a microseismic at depth
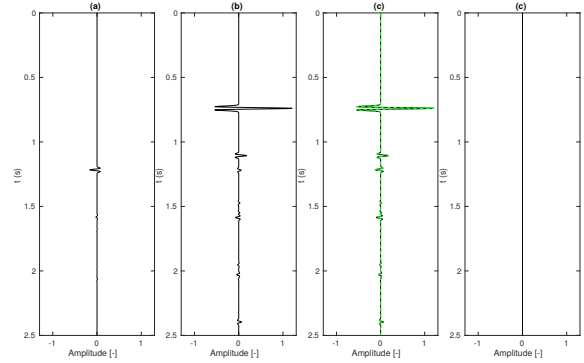
Figure 5: *Comparison of the retrieved wavefields in black with the reference wavefields in dashed green. The retrieved (a) upgoing field and (b) downgoing field. (c) Comparison of the full Green's function of the reference wavefield from Fig.2-d, in dashed green, and the sum of the wavefields in (a) and (b), in solid black. (d) Error between the wavefields in (c)*

is measured at the surface, source-receiver reciprocity could be used to use the receivers at the surface as sources and the source of the event at depth as a receiver, mimicking the situation of a downhole receiver in a borehole. The decomposed wavefield themselves can be used for a variety of purposes. All of our examples in this abstract were in 1D, but currently we are working to extend this work to 2D.